Moiré butterflies in twisted bilayer graphene

R. Bistritzer and A. H. MacDonald
Department of Physics, The University of Texas at Austin, Austin, Texas 78712 USA
(Received 27 January 2011; revised manuscript received 23 June 2011; published 27 July 2011)

The Hofstadter butterfly spectral patterns of lattice electrons in an external magnetic field yield some of the most beguiling images in physics. Here we explore the magnetoelectronic spectra of systems with moiré spatial patterns, concentrating on the case of twisted bilayer graphene. Because long-period spatial patterns are accurately formed at small twist angles, fractal *butterfly* spectra and associated magnetotransport and magnetomechanical anomalies emerge at accessible magnetic field strengths.

DOI: 10.1103/PhysRevB.84.035440 PACS number(s): 71.35.−y, 71.10.−w, 73.21.−b, 73.22.Gk

I. INTRODUCTION

The fractal Hofstadter spectrum is a canonical example of electronic structure in a system with incommensurate length scales, and has fascinated physicists and mathematicians for over a half a century.[1–7] The classic butterfly pattern is formed by the magnetic field dependent support of the eigenvalue spectrum of the Schrodinger equation for a near-neighbor hopping model on a square lattice. Similar but distinct[8] patterns describe the magnetospectrum of any two-dimensional (2D) system of Bloch electrons.

Quite generally magneto-Bloch Hamiltonians are block diagonalizable only when the magnetic flux through a 2D unit cell Φ is a rational multiple of the magnetic flux quantum Φ_0. For $\alpha \equiv \Phi_0/\Phi = p/q$ (p and q coprime) the spectrum consists of continuous sub-bands each containing an areal density of $B/q\Phi_0$, q times smaller than the usual semiclassical Landau level density. Because the x and y components of cyclotron orbit centers are canonically conjugate in a magnetic field,[9] smearing the periodic potential over the magnetic length scale $\ell = (\Phi_0/2\pi B)^{1/2}$, the fractal pattern of gaps within Landau levels becomes visible only when α is not too much larger than one. For atomic periodicity this condition is not met until the magnetic field strength exceeds laboratory scales by a factor of about 1000. In moiré systems,[10] however, the pattern period can easily exceed ℓ. Graphene moiré systems realize Hofstadter physics at fields of a few Tesla, without recourse to the difficult and potentially damaging photolithographic patterning previously used[11] to realize Hofstadter physics in the laboratory.

Because of the relatively weak forces between adjacent graphene layers, double layer graphene systems with a variety of different stacking sequences occur in bulk graphite,[12] epitaxially grown multilayer graphene,[13] and in mechanically exfoliated multilayers. [14] Relative twists between layers can also be created by folding a single layer.[15,16] The stacking arrangement in a two-layer system can be characterized by the twist angle θ, and by a relative translation $\mathbf{d}$. A variety of different aspects of twisted bilayer electronic structure have captured theoretical attention,[17–23] and been studied experimentally.[14,24,25]

For θ smaller than roughly 10°, the low-energy spectrum is faithfully described by a continuum model obtained via an envelope function approximation.[17,23] For small twist angles, this model shows that it is meaningful to describe the electronic structure in terms of Bloch bands for any θ even though the atomic network is periodic only for a discrete set of angles.[23] The Bloch bands in this description are intimately related to the moiré pattern clearly observed in scanning tunneling microscopy measurements.[13] The moiré period for bilayer graphene is $a/[\sin(\theta/2)]$ where a is graphene's lattice constant. Because a translation of one layer with respect to the other only shifts the moiré pattern, the electronic structure is virtually independent of $\mathbf{d}$ [23] except at large commensurate twist angles. In what follows, we therefore set $\mathbf{d}$ to zero.

The continuum limit of a π-band tight-binding model for the twisted bilayer yields a transparent physical picture in which Dirac cones are coupled by a position and sublattice dependent interlayer hopping operator $T(\mathbf{r})$ that captures the local coordination of the twisted honeycomb lattices. As we show below it is $T(\mathbf{r})$, and not a periodic potential, which is responsible for the moiré butterfly. Because the moiré unit cell area $\Omega_M \propto \theta^{-2}$, the flux through a moiré unit cell increases rapidly as the twist angle is reduced. As in the periodic potential case, gaps open within Landau levels for $\alpha \lesssim 1$. It turns out that $B[T] \approx 4(\theta^\circ)^2/\alpha$. Significant splitting of the isolated layer Dirac Landau levels therefore appear already at low magnetic fields for small θ.

We now derive the equations we use to evaluate the moiré butterfly spectrum at rational values of α, present numerical results for a typical twist angle, and discuss the magnetotransport and magnetomechanical anomalies that they imply.

II. HAMILTONIAN

The low-energy electronic structure of a twisted bilayer is well captured by the continuum model in which[23]

$$H = \begin{pmatrix} h(-\theta/2) & T(\mathbf{r}) \\ T^\dagger(\mathbf{r}) & h(\theta/2) \end{pmatrix}, \tag{1}$$

where $h = iv\sigma \cdot \nabla$ with $\sigma = (\sigma_x, \sigma_y)$ being the sublattice Pauli matrices of the single-layer graphene Hamiltonian, and

$$T(\mathbf{r}) = w \sum_j e^{-i\mathbf{q}_j \cdot \mathbf{r}} T_j \tag{2}$$

is the interlayer hopping matrix. Here

$$T_1 = \begin{pmatrix} 1 & 1 \\ 1 & 1 \end{pmatrix}, T_2 = \begin{pmatrix} e^{-i\phi} & 1 \\ e^{i\phi} & e^{-i\phi} \end{pmatrix}, T_3 = \begin{pmatrix} e^{i\phi} & 1 \\ e^{-i\phi} & e^{i\phi} \end{pmatrix}, \tag{3}$$

where $\phi = 2\pi/3$, $\mathbf{q}_1 = k_\theta(0, -1)$, $\mathbf{q}_2 = k_\theta(\sqrt{3}, 1)/2$, $\mathbf{q}_3 = k_\theta(-\sqrt{3}, 1)/2$, $k_\theta = 2k_D \sin(\theta/2) \approx k_D\theta$ with k_D being the

Dirac momentum and w the hopping energy. Estimates based on tight-binding models for AB bilayer graphene imply that $w \approx 110$ meV, however recent measurements suggest that w might be considerably smaller for some epitaxially grown layers.[26]

The AA entry of the T matrix is depicted in Fig. 1 (similar figures are obtained for the other entries of T). The direction and size of an arrow at position $\mathbf{r}$ correspond respectively to the phase of $T_{\rm AA}(\mathbf{r})$ and to its magnitude. The red dots mark the lattice associated with the moiré pattern[23] whereas the green circles mark the lattice on which $T(\mathbf{r})$ is periodic. Interestingly, the moiré unit cell area $\Omega_{\rm M} = 16\pi^2/\sqrt{3}k_\theta^2$ is six times larger than the area of the moiré pattern unit cell.

In the presence of a magnetic field it is convenient to work in the Landau gauge $\mathbf{A} = B(-y,0)$ and express the Hamiltonian in the representation of the basis states $|Ln\alpha y\rangle$ where $L = 1,2$ labels the layer, n is the Landau level index, $\alpha = A,B$ stands for the sublattice, and y is the guiding center coordinate. In terms of these basis states the intralayer part of the Hamiltonian

$$h(\theta) = -\omega_c \sum_{Lny} (e^{-i\theta}\sqrt{n+1}|Ln+1Ay\rangle\langle LnBy| + \text{H.c.}) \tag{4}$$

is diagonal in y, however the T_2 and T_3 interlayer hopping terms change y by $\pm\Delta$ where $\Delta = \sqrt{3}k_\theta\ell^2/2$. In the presence of a finite B the Hamiltonian therefore describes particles hopping on a set of one-dimensional chains. The Hamiltonian can be block-diagonalized in y by grouping guiding centers separated by integer multiples of Δ.

The guiding center chains become periodic when Φ_0/Φ is rational (or equivalently when $k_\theta\Delta/2 = 2\pi p/q$), allowing a second wave vector to be introduced. The corresponding basis functions are constructed by writing the y-guiding coordinate as $y = y_0 + (mq+j)\Delta$ and Fourier transforming with respect to m. The resulting magnetic Brillouin zone is

$$\{(k_1,k_2)|0 < k_1 = y_0/\ell^2 < \Delta/\ell^2, 0 < k_2 < 2\pi/q\Delta\}. \tag{5}$$

The Hamiltonian matrix in this magnetic Bloch representation has dimension $4q$ times the number of Landau levels retained. For each momentum in this zone

$$T(\mathbf{k}) = \sum_{nm\alpha\beta j} \left[T_j^{(0)}|2n\alpha j\rangle\langle 1m\beta j| + T_j^{(R)}|2n\alpha, j+1\rangle \times\langle 1m\beta j| + T_j^{(L)}|2n\alpha j-1\rangle\langle 1m\beta j|\right], \tag{6}$$

where $j = 0,1,\ldots,q-1$ (j is defined modulo q so that $|j = q\rangle = |j = 0\rangle$), and

$$\begin{aligned} T_j^{(0)} &= T_1 F_{nm}\left(\frac{\mathbf{q_1}\ell}{\sqrt{2}}\right) e^{-ik_\theta y_0} e^{-4\pi i \frac{p}{q} j}, \\ T_j^{(R)} &= T_2 F_{nm}\left(\frac{\mathbf{q_2}\ell}{\sqrt{2}}\right) e^{ik_2\Delta} e^{\frac{i}{2}k_\theta y_0} e^{i\pi\frac{p}{q}(2j-1)}, \\ T_j^{(L)} &= T_3 F_{nm}\left(\frac{\mathbf{q_3}\ell}{\sqrt{2}}\right) e^{-ik_2\Delta} e^{\frac{i}{2}k_\theta y_0} e^{i\pi\frac{p}{q}(2j+1)}. \end{aligned} \tag{7}$$

Here

$$F_{nm}(\mathbf{z}) = \sqrt{\frac{m!}{n!}}(-z_x + iz_y)^{n-m} e^{-\frac{z^2}{2}} \mathcal{L}_m^{n-m}(z^2) \tag{8}$$

for $n \geqslant m$ with $\mathcal{L}$ being the associated Laguerre polynomial. For $n < m$ the function F can be found using $F_{nm}(\mathbf{z}) = F^\star_{mn}(-\mathbf{z})$. Because $(k_\theta\ell)^2 = 8\pi p/\sqrt{3}q$, the inter-layer Hamiltonian depends only on p/q. In the absence of Landau level mixing the splitting of each Landau level into sub-bands is therefore determined only by α.

We now comment on the range of validity of our model. For the intralayer terms in Hamiltonian (1) we use the standard Dirac-like model, which is valid up to energies $\sim$1 eV. For the interlayer terms we use a continuum model that is valid when the local coordination between layers varies slowly on a lattice constant scale, i.e., when the moire period is long. Our model is therefore valid for energies within $\sim$1 eV of the Dirac point and rotation angles smaller than around 10°. As mentioned in the introduction we set $d = 0$ throughout this work. For incommensurate structures a translation has no influence on the spectrum (neglecting finite size effects). For commensurate angles for which the bilayer is crystalline a translation of one layer with respect to the other modifies the unit cell and does in principle influence the spectrum. However, such **d**-related corrections to the spectrum diminish as the size of the unit cell increases becoming negligible for $\theta \lesssim 10^\circ$. [22]

III. SPECTRUM

In the absence of interlayer coupling, the spectrum consists of degenerate Dirac Landau levels at energies $\pm\omega_c\sqrt{n}$, where $\omega_c = \sqrt{2}v/\ell$ is the cyclotron energy, and v is the graphene sheet Dirac velocity. Because of the layer degeneracy, gaps between Landau levels produce quantum Hall effects at odd,

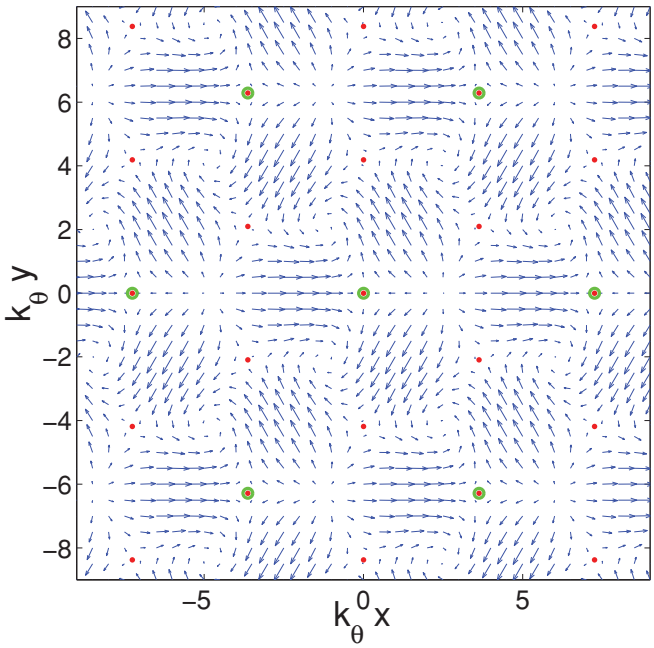

FIG. 1. (Color online) Moiré unit cell. The magnitude and phase of the AA hopping amplitude (represented by arrows) is plotted as a function of position (in units of k_θ^{-1}). The lattice that corresponds to the moiré pattern is marked by the red dots and the lattice on which the interlayer hopping Hamiltonian is periodic is denoted by the green circles. It is this second lattice that determines the moiré unit cell area $\Omega_{\rm M}$.

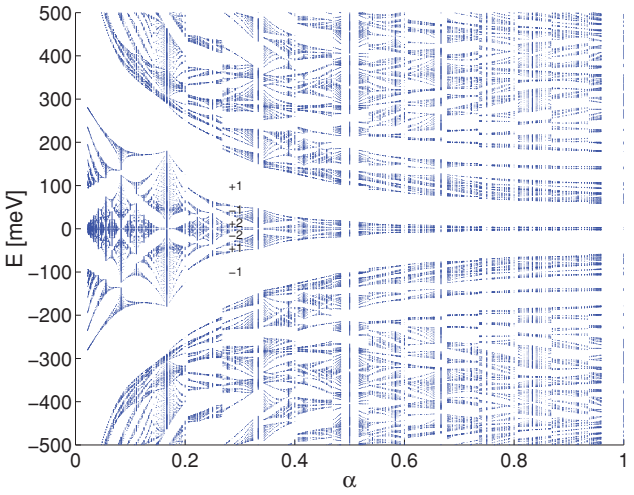

FIG. 2. (Color online) Spectrum support. The support of the spectrum as a function of α for $\theta = 2^\circ$ ($w = 110$ meV). The periodic interlayer hopping amplitude results in a Hofstadter-like sub-band structure. The integers denote the Hall conductivity associated with the larger energy gaps between $\nu = 1$ and $\nu = -1$ for $\alpha \approx 0.3$.

rather than half-odd,[27] integer filling factors. (Spin and valley degeneracy are left implicit throughout this article.) Coupling between the layers splits the Landau levels of both layers into q sub-bands and couples them together as illustrated in Fig. 2 for the $\theta = 2^\circ$ case. It is clear that interlayer coupling at strong fields completely alters the spectrum.

Inter-Landau level transitions can significantly alter the electronic spectrum.[28,29] In the absence of a magnetic field two momentum states are effectively coupled if their energy difference is of order of $E_\Lambda = \max(vk_\theta, w)$ or less. The same criteria holds also in the presence of a magnetic field. The $n = 0$ Landau level therefore couples most strongly to the $n_0 \approx (E_\Lambda/\omega_c)^2$ Landau level. In our calculations we retain $\sim 2n_0$ Landau levels[30] in order to obtain spectra that are accurate near the Dirac point. Comparing Fig. 2 with results obtained neglecting Landau level mixing (not shown) we find that, as expected, inter-Landau level hopping is increasingly important as the magnetic field is reduced and as the energy is increased.

Because $\alpha \propto \theta^2/B$ the sub-band structure becomes more conspicuous as θ is reduced. On the other hand, the band structure for very small twist angles does not have simple Dirac character even at $B = 0$.[23] In Fig. 2 we show the support of the spectrum for the intermediate case $\theta = 2^\circ$. As the magnetic field is increased (i.e., as α is decreased) all the gaps widen. The terminology of Landau level splitting is useful as long as the single layer Landau levels do not overlap. Minigaps as large as 10 meV open up within the $n = 0$ Landau level for $B \approx 40$ T. When any one of the three tunneling processes T_j is present alone, the $n = 0$ Landau level splits into two precisely degenerate components. The relatively large gap at the $\nu = 0$ neutrality point which is present over a wide range of α in Fig. 2 is a remnant of this behavior which often remains when all three hopping processes are restored.

IV. HALL CONDUCTIVITY

Since the pioneering work of Thouless *et al.*[5] it has been understood that the Hall conductivity σ_H (in units of e^2/h) is a topological number that must be quantized when the chemical potential lies in an energy gap. Although the support of the spectrum as a function of field has a fractal structure, gaps in the spectra can exist continuously over finite ranges of field. The Landau level filling factors ν at which gaps appear are characterized by two topological integers σ_H and s[5,31] which satisfy

$$\nu = \sigma_H + s\alpha. \tag{9}$$

Here

$$s = -\frac{\Omega}{A}\left(\frac{\partial N}{\partial \Omega}\right)_B = \frac{\Omega}{A}\frac{\partial^2 \mathcal{F}}{\partial \mu\, \partial \Omega}, \tag{10}$$

A is the sample's area, Ω is the area of the unit cell, N is the number of electrons in states below that gap, μ is the chemical potential, and $\mathcal{F}$ is the grand-canonical potential. As a function of ν and α, the Diophantine equation (9) has an infinite number of solutions: $(s,\sigma_H) = (s_0 - mq, \sigma_0 + mp)$, where (s_0,σ_0) is some particular solution and m is any integer. The topology of the classic Hofstadter spectrum corresponds to the rule[5] that s should be as small as possible. For general models there are exceptions to this rule[8] that alter the connectivity of spectral gaps. For the moiré butterfly we therefore find s and σ_H numerically by plotting the energy gaps as a function of ν and α. The linear dependence assured by Eq. (9) allows a straightforward identification of σ_H as the intercept of gap lines with the $\alpha = 0$ axis and of s as the gap-line slope. In Fig. 3 the energy gaps are plotted for $\theta = 2^\circ$.

Using Fig. 3 we can identify the topological quantum numbers for every gap in Fig. 2, as illustrated for some of the larger gaps that appear near $\alpha \approx 0.3$. The integers depicted in Fig. 2 specify the quantized Hall conductance in the large gaps

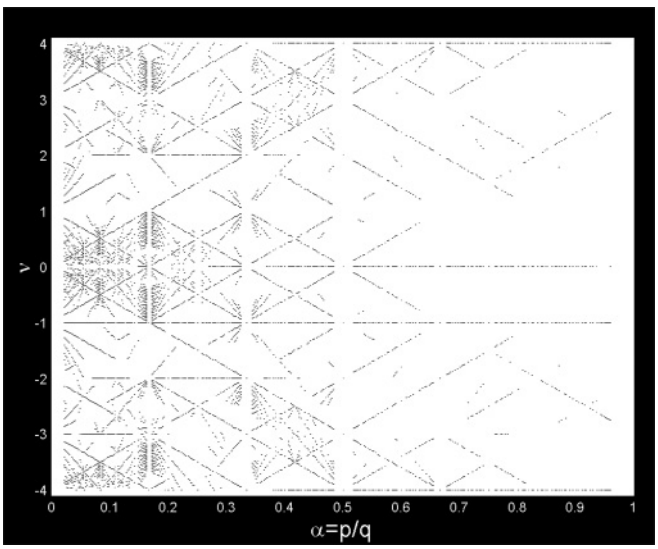

FIG. 3. Hall conductivity. The energy gaps are depicted as a function of filling factor ν and p/q for $\theta = 2^\circ$ ($w = 110$ meV). The conspicuous straight lines satisfy the Diophantine gap equation (9) and determine both σ_H and s. The Hall conductivity corresponds to the intercept of the line with the y-axis whereas s is given by its slope.

which appear between $\nu = 1$ and $\nu = -1$. As the electronic density is varied the quantized Hall conductivity follows the nonmonotonic variation $+1, -1, +2, -2, +1, -1$.

V. SUMMARY

The moiré pattern formed in twisted double layer graphene systems is akin to an atomic periodic potential. In the presence of a magnetic field the twisted bilayer possesses a Hofstadter-like energy spectrum. Because the area of the moiré unit cell is very large at small twist angles sub-bands can appear in twisted bilayers at relatively low magnetic fields that are accessible in a laboratory.

Two topological integers are associated with each energy gap in the spectrum. The first is related to the Hall conductivity. For twisted bilayers, we find that the second number has an electromechanical origin. As evident from Eq. (10), the quantum number s can be associated with the chemical potential dependence of a rotational torque. Measurement of this electromechanical quantum number presents an interesting challenge to experiment.

Our theory has intriguing consequences for magnetotransport in double layers grown using chemical vapor deposition (CVD). This type of sample is polycrystalline in nature, characterized by graphene flakes of various sizes that are misoriented relative to one another. A double-layer CVD grown structure will therefore be characterized not by a single twist angle but by a set of θ's. In the presence of a magnetic field the Hall conductivity of each domain will depend on B *and* on the particular twist angle of the domain. Because different grains will in general have different Hall conductivities, chiral currents will flow along most grain boundaries.

We note that the considerations presented here do not account for electron-electron interactions.[32] As in the case of patterned semiconductor quantum wells, fractional quantum Hall states with fractional charge and statistics are possible.[33,34] The large minigaps depicted in Fig. 2 and the typical high mobilities of graphene multilayers are favorable for the experimental observation of these fractional states in exfoliated double-layer graphene samples.

Over the past decades many interesting theoretical predictions were made regarding the Hofstadter spectrum. As this work shows twisted double-layer graphene systems may enable to bridge between these predictions and experiments.

ACKNOWLEDGMENTS

We acknowledge a helpful conversation with João Lopes dos Santos, and thank Gene Mele for pointing out the difference between the moiré pattern and the $T(\mathbf{r})$ periodicity. This work was supported by Welch Foundation grant no. F1473 and by the NSF-NRI SWAN program.

[1] P. G. Harper, Proc. Phys. Soc. London, Sect. A **68**, 874 (1955).
[2] M. Ya. Azbel', Zh. Eksp. Teor. Fiz. **46**, 939 (1964) [Sov. Phys. JETP **19**, 634 (1964)].
[3] D. R. Hofstadter, Phys. Rev. B **14**, 2239 (1976).
[4] P. Streda, J. Phys. C **15**, L1299 (1982).
[5] D. J. Thouless, M. Kohmoto, M. P. Nightingale, and M. den Nijs, Phys. Rev. Lett. **49**, 405 (1982).
[6] A. H. MacDonald, Phys. Rev. B **28**, 6713 (1983).
[7] O. Gat and J. Avron, New J. Phys. **5**, 44 (2003).
[8] A. H. MacDonald, Phys. Rev. B **29**, 3057 (1984).
[9] A. H. MacDonald, in *Physique Quantique Mésoscopique, Les Houches Session LXI*, edited by E. Akkermans *et al*. (Elsevier, Amsterdam, 1995).
[10] I. Amidror, *The Theory of the Moire Phenomenon*, Vol. I (Springer, London, 2009).
[11] C. Albrecht, J. H. Smet, K. vonKlitzing, D. Weiss, V. Umansky, and H. Schweizer, Phys. Rev. Lett. **86**, 147 (2001).
[12] Z. Y. Rong and P. Kuiper, Phys. Rev. B **48**, 17427 (1993).
[13] J. Hass, F. Varchon, J. E. Millan-Otoya, M. Sprinkle, N. Sharma, W. A. deHeer, C. Berger, P. N. First, L. Magaud, and E. H. Conrad, Phys. Rev. Lett. **100**, 125504 (2008).
[14] A. Luican *et al*., Phys. Rev. Lett. **106**, 126802 (2011).
[15] H. Schmidt, T. Ludtke, P. Barthold, and R. J. Haug, Phys. Rev. B **81**, 121403(R) (2010).
[16] K. Kwanpyo *et al*., e-print arXiv:1012.5426.
[17] J. M. B. Lopes dos Santos, N. M. R. Peres, and A. H. Castro Neto, Phys. Rev. Lett. **99**, 256802 (2007).
[18] S. Shallcross, S. Sharma, E. Kandelaki, and O. A. Pankratov, Phys. Rev. B **81**, 165105 (2010).
[19] G. Trambly de Laissardière, D. Mayou, and L. Magaud, Nano Lett. **10**, 804 (2010).
[20] E. S. Morell, J. D. Correa, P. Vargas, M. Pacheco, and Z. Barticevic, Phys. Rev. B **82**, 121407(R) (2010).
[21] E. J. Mele, Phys. Rev. B **81**, 161405(R) (2010).
[22] R. Bistritzer and A. H. MacDonald, Phys. Rev. B **81**, 245412 (2010).
[23] R. Bistritzer and A. H. MacDonald, doi: 10.1073/pnas.1108174108.
[24] G. Li *et al*., Nature Phys. **6**, 109 (2010).
[25] A. H. MacDonald and R. Bistritzer, Nature **474**, 453 (2011).
[26] J. Hicks *et al*., Phys. Rev. B **83**, 205403 (2011).
[27] K. S. Novoselov *et al*., Science **315**, 1379 (2007).
[28] A. H. MacDonald, Phys. Rev. B **30**, 4392 (1984).
[29] M. C. Geisler, J. H. Smet, V. Umansky, K. vonKlitzing, B. Naundorf, R. Ketzmerick, and H. Schweizer, Phys. Rev. Lett. **92**, 256801 (2004).
[30] When the Landau level cutoff index has the same value on both sublattices, an artificial zero-energy state appears in the spectrum. It is essential that on both layers the cutoff indices of the two sublattices differ by one. This approach shifts numerical errors to high energies.
[31] I. Dana, Y. Avron, and J. Zak, J. Phys. C **18**, L679 (1985).
[32] J. E. Avron and L. G. Yaffe, Phys. Rev. Lett. **56**, 2084 (1986).
[33] A. Kol and N. Read, Phys. Rev. B **48**, 8890 (1993).
[34] D. Pfannkuche and A. H. MacDonald, Phys. Rev. B **56**, R7100 (1997).